**Marine Biodiversity**
December 2019, Volume 49, Issue 6, Pages 2571-2586
https://doi.org/10.1007/s12526-019-00987-3
https://archimer.ifremer.fr/doc/00511/62292/



# *Xylocythere sarrazinae*, a new cytherurid ostracod (Crustacea) from a hydrothermal vent field on the Juan de Fuca Ridge, northeast Pacific Ocean, and its phylogenetic position within Cytheroidea

Tanaka Hayato [1, *] , Lelièvre Yann [2, 3], Yasuhara Moriaki [4]

[1] Tokyo Sea Life ParkTokyo, Japan
[2] Ifremer Centre de Bretagne, REM/EEP, Laboratoire Environnement ProfondPlouzane, France
[3] Département de Sciences BiologiquesUniversité de MontréalMontreal, Canada
[4] School of Biological Sciences and Swire Institute of Marine ScienceThe University of Hong KongHong Kong, China

* Corresponding author : Hayato Tanaka, email address : Cladocopina@gmail.com

**Abstract :**

This paper described *Xylocythere sarrazinae* sp. nov. (Ostracoda: Cytheroidea: Cytheruridae: Eucytherurinae), collected at 2196 m depth from the Grotto hydrothermal edifice (Main Endeavor Field, Juan de Fuca Ridge) in the northeastern Pacific Ocean. This new species was found living in association with *Ridgeia piscesae* tubeworm assemblages. It is the second representative of *Xylocythere* described from such vents. *Xylocythere sarrazinae* sp. nov. is easily distinguished from the seven described species of *Xylocythere* by the surface ornamentations of its carapace, with the most similar species to it being *Xylocythere pointillissima* Maddocks & Steineck, 1987. However, *Xylocythere sarrazinae* sp. nov can be distinguished from *X. pointillissima* based on the following characters: having a subsquare basal capsule outline, a spatulate upper ramus, a flattened distal lobe of the male copulatory organ, and having 15 maxillula branchial plate setae. We found that one specimen of this new species had multiple spherical objects associated with the internal openings of its pore clusters. These objects were quite similar in shape to that of chemoautotrophic bacteria, which were previously reported from the outer surfaces of pore clusters in other *Xylocythere* species. Finally, we provided a preliminary phylogenetic analysis of this new species based on 18S rRNA gene sequences to determine the phylogenetic position of the subfamily Eucytherurinae within the superfamily Cytheroidea. This analysis revealed that *Xylocythere* (Eucytherurinae) may be the most ancestral lineage among the Cytheruridae and identified paraphyletic relationships among the three subfamilies within Cytheruridae. This result supported certain previous studies' conclusions based on morphology and fossil records.

**Keywords** : Chemosynthetic habitat, Crustacea, Eucytherurinae, Meiofauna, Pore clusters

## Introduction

Ostracods are tiny crustaceans covered by a calcified carapace with two valves. They are important representatives of the meiofaunal compartment. They occur in a wide variety of aquatic environments including deep-sea chemosynthetic habitats. According to a recent review on living and fossil ostracods from chemosynthetic ecosystems (Karanovic and Brandão 2015), most deep-sea species have been described from the eastern Pacific Ocean (Kornicker 1991; Kornicker and Harrison-Nelson 2005; Maddocks 2005). Additionally, several species left in open nomenclature have been reported from the equatorial Pacific and northern Atlantic oceans (van Harten 1992, 1993; Degen et al. 2012; Zeppilli and Danovaro 2012). Recently, the first ostracod species from hydrothermal vents in the western Pacific Ocean was described by Tanaka and Yasuhara (2016). Regardless of their recent distribution, fossil records of vent ostracods trace back to the middle Devonian (Olempska and Belka 2010).

In this paper, we describe a new ostracod species belonging to the genus *Xylocythere* (Maddocks and Steineck, 1987) that was recently discovered on the Juan de Fuca Ridge, northeastern Pacific. The type species of this genus, *Xylocythere turnerae* Maddocks and Steineck, 1987, was collected from deep-sea experimental wood falls at approximately 3500 m depth deployed on the southeast of Woods Hole, Massachusetts (USA). Simultaneously, three other *Xylocythere* species were also described from the Tongue of the Ocean (Bahamas), off Sainte Croix (Virgin Islands) and from the Panama basin (Maddocks and Steineck 1987) (see Fig. 1 and Table 1). Five years later, van Harten (1992) discovered a

*Xylocythere* species from a vent field of the East Pacific Rise and discussed the relationships between deep-sea wood-island habitats and vent fauna with regard to their distribution and trophic ecology. Subsequently, this species was formally described as *Xylocythere vanharteni* based on newly collected specimens (Maddocks 2005). Thus, five living *Xylocythere* species are known and all of them are endemic to chemosynthetic habitats. Additionally, two fossil species are known, namely *Xylocythere producta* (Colalongo and Pasini, 1980), from the Middle Miocene to the Early Pleistocene (Colalongo and Pasini 1980; Dall'Antonia 2003), and *Xylocythere carpathica* Szczechura, 1995, from the Middle Miocene (Szczechura 1995, 2000). Several unnamed fossil species of *Xylocythere* were also reported from the Late Eocene to the Holocene (Steineck et al. 1990; Corrège 1993; Kiel and Goedert 2006; Bergue and Coimbra 2008; Yasuhara et al. 2009; Machian-Castillo et al. 2014). Notably, the oldest *Xylocythere* fossil (Late Eocene) was recorded as a member of wood-fall assemblages (Kiel and Goedert 2006). Their wide geographical distribution and bathymetric range (Fig. 1 and Table 1) imply ancient origins. This study describes a new *Xylocythere* species based on the morphology of the carapace and soft parts. This is the second representative of *Xylocythere* coming from an hydrothermal vent field. The objective of this study is to provide the detailed morphological description of this new species of *Xylocythere*, which was found at 2196m depth on the Grotto hydrothermal edifice located on the Juan de Fuca ridge northeast Pacific. The new species was found living in association with *Ridgeia piscesae* tubeworm assemblages, in areas of low fluid emissions. We also provide a preliminary phylogenetic analysis of this new species based on nearly complete 18 rDNA sequence in order to detect the phylogenetic position of subfamily Eucytherurinae within superfamily Cytheroidea.

## Materials and Methods

### Study site

The 90 km Endeavour segment, located on the northern part of the Juan de Fuca Ridge (JdFR), is a hydrothermally active region harboring five major hydrothermal vent fields (Kelley et al. 2012). Among these, the Main Endeavour Field (MEF) (Fig. 2) includes Grotto (47.949292N, 129.098433W), a 10 m high active hydrothermal sulfide vent cluster located at a depth of 2196 m. This large complex covers a surface area of 450 $m^2$, and forms a cove with an opening to the north (Xu et al. 2014). Located in the Endeavour Hydrothermal Vent Marine Protected Area (MPA), this site was selected as a target for sensor deployment as part of the cabled deep-sea observatory of Ocean Networks Canada (ONC) to study and monitor the temporal dynamics of deep-sea vent ecosystems. Like many other sulfide structures within the MEF, Grotto is colonized by a mosaic of faunal assemblages (Sarrazin et al. 1997), including the low-flow assemblages of the tubeworm *Ridgeia piscesae* Jones, 1985 and their associated fauna.

### Sampling

The *Ocean Networks Canada Expedition 2015: Wiring the Abyss* cruise was conducted from aboard the *R/V Thomas G. Thompson* vessel with the Remotely Operated Vehicle (ROV) *Jason* from August 25 to September 14 2015. The specimens of ostracods examined were collected on September 7 2015, within two samples of *R. piscesae* tubeworms taken from the Grotto edifice. The locations of the two samples were as follows: dive J0831-S1 (47.949292N, 129.098433W, 2196 m depth) and dive J0831-S3 (47.949302N, 129.098491W, 2196 m depth). Details of the sampling methods used can be found in Lelièvre et al. (2018). After bringing the faunal samples aboard, the

siboglinid tubeworm assemblages were washed over stacked sieves (with 250 µm, 63 µm, and 20 µm mesh sizes). Ostracod specimens were picked out from the remnants in the 250 µm sieves and preserved in 96% ethanol. A total of 35 individuals of *Xylocythere* were randomly extracted from the two samples (dive J0831-S1 and -S3) and examined for the present taxonomic study. The remaining ostracod specimens were used in isotopic analyses and biodiversity studies (Lelièvre et al. 2018).

**Morphology**

The collected ostracod specimens were fixed in 96% ethanol and preserved at room temperature for description and DNA extraction. The soft parts were separated from the valves and dissected using fine needles under a stereo-binocular microscope (SZH 10, OLYMPUS). The valves were preserved on a cardboard cell slide and the soft parts mounted in a gum-chloral medium, Neo-Shigaral (Shiga Konchu Fukyusha, Japan), on glass slides. The specimens were then observed and sketched using a transmitted-light binocular microscope (BX 50, OLYMPUS) with a differential interference contrast system and a camera Lucida. The valves were washed with distilled water and gold-coated by an Ion sputtering device (JFC-1100, JEOL). The valves were then observed by scanning electron microscopy (SEM; JSM-5600LV, JEOL). The type series was deposited in the collection of the University Museum, The University of Tokyo (UMUT) with the prefix 'UMUT RA'. Terminology on appendage and carapace morphologies is adapted from Maddocks (2005).

**DNA extraction, amplification and sequencing**

Total DNA extraction from holotype (UMUT RA32930) was performed using the DNeasy Blood and Tissue Kit (Qiagen, USA) following the manufacturer's protocol. Morphological voucher was prepared following by Tanaka and Ohtsuka (2016) and deposited in the UMUT.

Nearly complete sequence of the nuclear 18S rRNA gene was PCR amplified using the eukaryotic primers (Moon-van der Staay et al. 2000). The 25 µl reaction contained 0.125 µl of TaKaRa Ex Taq HS (TAKARA BIO Inc., Japan), 2.5 µl of 10×Ex Taq buffer, 2 µl of dNTP mix, 1 µl of each primer (5 pmoles each), 5 µl of template DNA, and 13.375 µl sterilized distilled water. The PCR protocol consisted of an initial denaturation step at 95 °C for 2 min, followed by 40 cycles of denaturation at 98 °C for 10 s, annealing at 52 °C for 30 s, extension at 72 °C for 2 min, and a final extension at 72 °C for 10 min. Quantity and length of the PCR products were checked by 1% agarose S (Nippon Gene, Japan) gel electrophoresis and stained with ethidium bromide. The products were purified for sequencing using a FastGene Gel/PCR Extraction Kit (NIPPON Genetics Co, Ltd, Japan), according to the manufacturer's protocol. Sequencing was performed by the Macrogen Japan Corp. (Tokyo, Japan) with the same primers as those used for PCR amplification.

**Sequence analysis and phylogenetic reconstruction**

A homology search of 18S rDNA sequence was performed by BLAST (Altschul et al. 1990, 1997) with the megablast program from the National Center for Biotechnology Information (NCBI, http://blast.ncbi.nlm.nih.gov/Blast.cgi). All of already existing 44 sequences of 18S rRNA gene of superfamily Cytheroidea Baird, 1850 and two outgroup sequences [*Neonesidea oligodentata* (Kajiyama, 1913), Bairdioidea Sars, 1866, AB076615 and *Heterocypris*

*incongruens* (Ramdohr, 1808), Cypridoidea Baird, 1845, EU370424] were downloaded from GenBank at May 2019. The sequences were aligned with MAFFT v. 7.310 (Katoh et al. 2002, 2005; Katoh and Standley 2013) using the L-INS-i algorithm. The ambiguous regions of the aligned sequences were detected and deleted using GBLOCKS 0.91b (Castresana 2000). Phylogenetic analyses were performed with the maximum likelihood (ML) and Bayesian inference (BI) methods using in PhyML v. 3.0 (Guindon and Gascuel 2003; Guindon et al. 2010) and MrBayes v. 3.2.2 (Ronquist and Huelsenbeck 2003), respectively. The jModelTest v. 2.1 (Darriba et al. 2012) for ML and MrModeltest v. 2.3 (Nylander 2004) for BI were used to find the best-fit evolutionary model for the present data set under the Akaike information criterion (AIC, Akaike 1974). For ML, the bootstrap values (Felsenstein 1985) were calculated with 1000 replications. For the BI method, four Markov chains were run for 1,000,000 generations, and were sampled every 100 generations. The convergence was assessed by using Tracer v1.6 (Rambaut et al. 2014). The first 2,500 samples from each run were discarded as burn-ins.

## Results

### Taxonomy

Subclass Podocopa Sars, 1866

Order Podocopida Sars, 1866

Superfamily Cytheroidea Baird, 1850

Family Cytheruridae Müller, 1894

Subfamily Eucytherurinae Puri, 1984 (emend. Maddocks and Steineck, 1987)

Genus *Xylocythere* Maddocks and Steineck, 1987

***Xylocythere sarrazinae* sp. nov.**

(Figs 4–9)

urn:lsid:zoobank.org:act:66E0D33D-CAB8-4C4F-8758-D7E95A7CAC69

Material examined. Holotype: adult male (UMUT RA32930), right valve length without anterior spines 548 μm, height 247 μm, left valve length 556 μm, height 254 μm, soft parts mounted on a glass slide and valves preserved in a micropalaeontological slide. Paratypes: 6 adult males (UMUT RA32931–32936) and 4 adult females (UMUT RA32937–32940).

Type locality. The holotype specimen and the paratypes were collected from the Grotto edifice of the Juan de Fuca Ridge, northeast Pacific (dive J0831-S1; 47.949292, -129.098433; depth 2196 m).

**Diagnosis.**

Carapace, elongate-ovoid. Surface nearly smooth and covered with numerous pore clusters. Two wedge-shaped denticles present at mid-height on the anterior margin of each valve. Male copulatory organ; copulatory process very short, bending dorsally; distal process, lamelliform bending ventrally with flattened distal end and one thin small process; upper ramus spatulate shaped; lower ramiform appendage with one short seta located distally.

**Description.**

**Adult male**

Carapace (Figs 4; 5a–d, g; 6). Size difference in length and height between left and right valves inconspicuous (Table 2). Both left and right valves of male slightly smaller than valves of female (Table 2; Fig 3). Elongate-ovoid outline, no conspicuous caudal process. Surface nearly smooth and covered with numerous pore clusters (Fig. 5a, b). Simple sensillum pores with rims locating on anterior and posterior region and without rims locating within muri. A prominent, posteriorly-directed postero-ventral spine present on the lateral surface of each valve (Figs 4; 5a, b). Two wedge-shaped denticles present at mid-height on the anterior margin of each valve (Fig. 5a). In dorsal view, carapace elongated-ovate with greatest thickness located slightly behind mid-length. Marginal infold broad (Fig. 5c, d). In interior view, numerous pore clusters visible (Fig. 5c, d). Adductor muscle scars four in vertical row (Figs 4; 6h). Hingement modified merodont-entomodont (Fig. 6a, b); left valve with deep sockets as anterior and posterior elements (Fig. 6c, e); right valve with kidney-shaped prominent terminal teeth as anterior and posterior elements (Fig. 6d, f); several crenulations developing at both ends of the median elements (Fig. 6c–f); middle part of median elements smooth bar.

Antennula (Fig. 7a). Six articulated podomeres, slender. First podomere bare. Second podomere with one seta on middle of posterior margin and setulae on anterior margin. Third podomere with one setulous seta on antero-distal end and setulae on anterior margin. Fourth podomere with two setae on antero-distal end and one seta on postero-distal end. Fifth podomere with three setae on antero-distal end and one seta on postero-distal end. Sixth podomere with two setae and one blunt tipped seta (aestetasc) on distal end.

Antenna (Fig. 7b). Five articulated podomeres. First podomere (basis) with one long four-segmented exopodite (spinneret seta). Second (first endopodite) podomere with two setae on postero-distal end. Third (second endopodite)

podomere with two setae on posterior end. Fourth podomere (third endopodite) with one slender spatulate seta on lateral surface of proximal part, one seta in middle of anterior margin, and one short stout seta on postero-distal part. Fifth (fourth endopodite) podomere with one short simple postero-distal seta and one stout distal claw.

Mandibula (Fig. 7c–e). Coxa with one long setulous dorsal seta. Coxal endite consisting of eight teeth (Fig. 7e). Palp consisting of four podomeres. First podomere (basis) with one long seta (exopodite) near proximal end and one long seta on ventro-distal end (Fig. 7d). Second podomere (first endopodite) with three setae ventro-distal end. Third podomere (second endopodite) with two setae on ventro-distal end and four setae on dorsal middle margin. Fourth podomere (third endopodite) with two setae on distal end.

Maxillula (Fig. 7f–j). Branchial plate (exopodite) with 15 plumose setae and two reflexed setae (Fig. 7f). Basal podomere with one palp (endopodite) and three endites (Fig. 7g). Palp consisting of two articulated podomeres: first podomere (first endopodite) with five distal setae; second podomere (second endopodite) very small, with two distal setae (Fig. 7g). Endites: dorsal one with five setae (Fig. 7h); middle one with four setae (Fig. 7i); ventral one with five setae (Fig. 7j).

Fifth limb (Fig. 8a). Four articulated podomeres. First podomere with one setulous and one stout postero-lateral setae, one long antero-lateral seta and two antero-distal setae. Second podomere with one short antero-distal seta. Third podomere bare. Fourth podomere with one distal claw.

Sixth limb (Fig. 8b). Four articulated podomeres. First podomere with two setulous setae on anterior middle margin, one stout postero-lateral seta, and one antero-distal seta. Second podomere with one antero-distal seta. Third podomere bare. Fourth podomere with one distal claw.

Seventh limb (Fig. 8c). Four articulated podomeres. First podomere with one setulous antero-distal seta. Second podomere with one setulous antero-distal seta. Third podomere bare. Fourth podomere with one long distal claw with small spines on distal area.

Brush-shaped organ (Fig. 8d). Consisting of two branches each with 8 setae on distal margin.

Head capsule (Fig. 8e). Sub-circular in lateral view. One paired rake-shaped structure in atrium space.

Male copulatory organ and posterior body (Fig. 9a). Basal capsule in lateral view sub-square tapering distally. Copulatory process very short, bending dorsally (cp). Distal process (dp), lamelliform bending ventrally with flattened distal end and one thin small process. Upper ramus (ur) spatulate shaped. Lower ramiform appendage (lra) with one short seta originating distally. Furca with two setulous setae.

**Adult female**

Carapace (Fig. 5e, f, h). Both left and right valves of female slightly larger than valves of male (Table 2; Fig 3).

Female copulatory organ and posterior body (Fig. 9b). Sclerotized framework of paired genital openings circular (right genital opening shown in figure). Posterior body with one stout long and two medium setulous setae on ventral margin, and post-abdominal bristle with rows of setulae.

**Distribution**

Only recorded from the type locality.

**18S rDNA sequence**

From holotype (UMUT RA32930), 1792 bp of the 18S rRNA gene sequence of *Xylocythere sarrazinae* sp. nov. was obtained and is available in the DNA Data Bank of Japan/European Molecular Biology Laboratory/NCBI databases under the accession number LC380020.

**Etymology**

The new species is named in honor of Dr. Jozée Sarrazin (Ifremer: Institut Français de Recherche pour l'Exploitation de la Mer) for her longtime contribution to deep-sea research and particularly, to vent ecology.

**Molecular phylogenetic analysis**

The alignment dataset of 45 sequences of Cytheroidea and two out-groups contained 1452 bp, including 488 variable sites. jModelTest identified GTR+I+G (proportion of invariable sites = 0.45, gamma shape=0.50) as the best-fit model under AIC (Akaike, 1974). The molecular phylogenetic analysis performed in this study based on 18S rDNA sequences indicates that the Family Cytheruridae and Subfamily Cytherurinae may be paraphyletic. Species of Cytherurinae join the same clade as Paradoxostomatidae, moderately supported by bootstrap value (79) and Bayesian posterior probability (1.00). (Fig. 10). Although we newly include Cytheroisinae sp. as representatives of subfamily Cytheroisinae (family Paradoxostomatidae), general topology was already demonstrated by previous molecular phylogenetic analyses (Yamaguchi, 2003). Our analyses showed that *Xylocythere sarrazinae* sp. nov.

(Eucytherurinae) is the most basal of all included cytherurids with strong nodal support (bootstrap value = 100, Bayesian posterior probability = 1.00).

**Discussion**

*Xylocythere sarrazinae* sp. nov. is easily distinguished from all described species of *Xylocythere* except for *X. pointillissima* Maddocks and Steineck, 1987. The surface ornamentation of *Xylocythere sarrazinae* sp. nov. is weak and smooth, in contrast with that of *X. trunerae* Maddocks and Steineck, 1987, *X. rimosa* Maddocks and Steineck, 1987, *X. tridentis* Maddocks and Steineck, 1987, *X. vanharteni* Maddocks, 2005, *X. producta* (Colalongo and Pasini, 1980), and *X. carpathica* Szczechura, 1995, which all show distinctly reticulated surface ornamentation on their carapaces. Other small differences also exist between *Xylocythere sarrazinae* sp. nov. and the seven other species cited above, as described in the following sentences. (1) The morphology of the male copulatory organ differs between *X. trunerae* and *X. sarrazinae* sp. nov. in that: the outline of the basal capsule is sub-circular in the former species, while it is sub-square in the latter; the upper ramus is conical in the former species and spatulate in the latter; and the tip of the distal lobe is tapered distally in the former species, while it is flattened in the latter. (2) *Xylocythere rimosa* differs from *X. sarrazinae* sp. nov. because it has a fairly large carapace that is more coarsely reticulated on its exterior surface. (3) *Xylocythere tridentis* has three large, wedge-shaped denticules located on the anterior margin of the carapace, while *X. sarrazinae* sp. nov. has only two denticules there that are much smaller. (4) *Xylocythere vanharteni* has a large, broad, sinuously curved upper ramus on the male copulatory organ, while the shape of upper ramus is spatulate in *X. sarrazinae* sp. nov. (5, 6) The two fossil species, *Xylocythere producta* and *X. carpathica*, have much more elongated, wedge-shaped carapaces in lateral view

compared to that of *X. sarrazinae* sp. nov. (7) Finally, *Xylocythere sarrazinae* sp. nov. has a similar morphology to that of *X. pointillissima* Maddocks and Steineck, 1987, which was described from an experimental wood-fall located off Sainte Croix (Virgin Islands, USA). However, *Xylocythere sarrazinae* sp. nov. and *X. pointillissima* can be distinguished based on the following characters: the outline of the basal capsule is sub-square in the former species versus sub-circular in the latter; the upper ramus is spatulate in *X. sarrazinae* sp. nov. versus conical in *X. pointillissima*; the tip of the distal lobe of the male copulatory organ is flattened in the former species versus rounded in the latter; and the number of setae on the maxillulal branchial plate is higher in former species than that in the latter (15 versus 12, respectively). In addition, the overall size of *X. sarrazinae* sp. nov. exceeds that recorded for *X. pointillissima* at all three locations (Maddocks and Steineck, 1987). Their spatial distributions also differ, as the former species was found in the northeast Pacific at 2196 m depth, while the latter was found in the western Atlantic at 4000 m depth.

In addition to *Xylocythere sarrazinae* sp. nov., we found another species of ostracods in the samples, which was *Euphilomedes climax* Kornicker, 1991 (Myodocopa: Philomedidae). The type locality of *E. climax* is the Upper Magic Mountain Vent located at 49°46'N, 130°116'W on the Explorer Ridge, northeast Pacific at a depth of 1700 m. *Euphilomedes climax* was also previously found on the Juan de Fuca Ridge, at the Long Time Observatory Vent, Endeavour segment (2250 m) and at the Hammond's Hell Vent, Axial Seamount (1570 m) (Kornicker, 1991), but it was reported from the Grotto edifice for the first time in the present study.

The subfamily Eucytherurinae that includes the genus *Xylocythere* is characterized by the presence of pore clusters on the carapace (Maddocks and Steineck, 1987). These pore clusters were initially defined by Maddocks and Steineck (1987). The occurrence of bacterial flocks around the exterior surface of pore clusters of *Xylocythere* was first described

by Van Harten (1993, Figs. 2A, C-D, G-I). These authors considered that it could represent an ‘exosymbiosis’. They also proposed that the pore clusters may contribute to the absorption of oxygen. In our new species *X. sarrazinae* sp. nov., multiple spherical structures were observed into the internal openings of the pore clusters, but only in one specimen (Fig. 6g). The shape and size (approximately 1.5 μm in diameter) of these structures were similar to those of the chemosynthetic bacteria observed to be symbionts in other invertebrates (Cavanaugh et al. 1981; Cavanaugh 1983; Van Dover et al. 2002). Additional samples would be required to verify the potential links between *X. sarrazinae* sp. nov. and such bacteria.

Finally, our phylogenetic analysis based on 18S rDNA sequences showed that *Xylocythere sarrazinae* sp. nov. (Eucytherurinae) is the most basal species of cytherurids, with strong nodal support for this conclusion (bootstrap value = 100; Bayesian posterior probability = 1.00). This result supports the taxonomic arrangement of there being three subfamilies within the family Cytheruridae (Cytherurinae, Cytheropterinae and Eucytherurinae), as proposed by Maddocks and Steineck (1987) and Mazzini and Gliozzi (2000), rather than two (Cytherurinae and Cytheropterinae), as proposed by Whatley and Boomer (2000). The fossil record of Cytheruridae extends back to the early Mesozoic or possibly the latest Permian. Species of the extant genera *Eucytherura* (Eucytherurinae) and *Cytheropteron* (Cytheropterinae) are known from the Triassic and Jurassic, respectively (Whatley and Boomer 2000). The basal position of *Xylocythere sarrazinae* sp. nov. in the molecular phylogenetic analysis performed in this study supports the hypothesized ancient origin of Eucytherurinae. Although our phylogenetic analysis is preliminary in nature because it was based on a single gene (18S) and limited taxon sampling, we used all of the available data that could possibly reconstruct the subfamily level phylogeny within Cytheroidea at the present time. The accumulation of

more genetic data than just 18S sequences and increased taxon sampling will allow the phylogenetic relationships within this family to be revealed more rigidly.

**Acknowledgements**

The authors thank the captain and crew of the *R/V Thomas G. Thompson* and the staff of Ocean Networks Canada and ROV's *Jason* pilots during the "*Ocean Networks Canada Expedition 2015: Wiring the Abyss*" cruise. We thank also Kim Juniper and the government of Canada in obtaining of works permit to study in Canadian waters (XR281, 2015). We are also grateful to Thomas Day for his assistance in sample sorting and Akira Tsukagoshi for providing the research facilities for taxonomy and molecular work. The work described in this article was partially supported by the grants from the Japan Society for the Promotion of Science for Young Scientists (No. 263700) (to HT), the Research Grants Council of the Hong Kong Special Administrative Region, China (project codes: HKU 17306014, HKU 17311316) (to MY). This research was part of Yann Lelièvre PhD thesis supervised by Legendre, P. (Université de Montréal) as well as Mariolaine Matabos and Jozée Sarrazin (Université de Bretagne Occidentale/Ifremer). His work was supported by a NSERC research grant to Pierre Legendre, Ifremer internal funds and a fellowship from the "Laboratoire d'Excellence" LabexMER (ANR-10-LABX-19). We would like to thank Editage (www.editage.jp) for English language editing.

**Funding:** This study was funded by the grants from the Japan Society for the Promotion of Science for Young Scientists (No. 263700) (to HT), the Research Grants Council of the Hong Kong Special Administrative Region, China (project

codes: HKU 17306014, HKU 17311316) (to MY), Ifremer internal funds and a fellowship from the "Laboratoire d'Excellence" LabexMER (ANR-10-LABX-19) (to YL) and NSERC research grant to Pierre Legendre.

**Conflict of Interest:** The authors declare that they have no conflict of interest.

**Ethical approval:** All applicable international, national, and/or institutional guidelines for the care and use of animals were followed by the authors.

**Sampling and field studies:** All necessary permits for sampling and observational field studies have been obtained by the authors from the competent authorities and are mentioned in the acknowledgements.

**References**

Akaike H (1974) A new look at the statistical model identification. IEEE Trans on Autom Control 19:716–723

Altschul SF, Gish W, Miller W, Myers EW, Lipman DJ (1990) Basic local alignment search tool. J Mol Biol 215:403–410

Altschul SF, Madden TL, Schäffer AA, Zhang J, Zhang Z, Miller W, Lipman DJ (1997) Gapped BLAST and PSI-BLAST: a new generation of protein database search programs. Nucleic Acids Res 25:3389–3402

Bergue CT, Coimbra JC (2008) Late Pleistocene and Holocene bathyal ostracodes from the Santos Basin, southeastern Brazil. Palaeontographica A 285:101–144

1 Castresana J (2000) Selection of conserved blocks from multiple alignments for their use in phylogenetic analysis. Mol
2 Biol and Evol 17:540–552
3 Cavanaugh CM, Gardiner SL, Jones ML, Jannasch HW, Waterbury JB (1981) Prokaryotic cells in the hydrothermal vent
4 tube worm *Riftia pachyptila* Jones: Possible chemoautotrophic symbionts. Science 213:340–342
5 Cavanaugh CM (1983) Symbiotic chemoautotrophic bacteria in marine invertebrates from sulphide-rich habitats. Nature
6 302:58–61
7 Colalongo ML, Pasini G (1980) La ostracofauna plio-pleistocenica della sezione Vrica in Calabria (con considerazioni
8 sul limite Neogene/Quaternario). B Soc Paleontol Ital 19:44–126
9 Corrège T (1993) The relationship between water masses and benthic ostracod assemblages in the western Coral Sea,
10 Southwest Pacific. Palaeogeogr Palaeoclimatol, Palaeoecol 105:245–266
11 Dall'Antonia B (2003) Miocene ostracods from the Tremiti Islands and Hyblean Plateau: biostratigraphy and description
12 of new and poorly known species. Geobis 36:27–54
13 Darriba D, Taboada GL, Doallo R, Posada D (2012) jModelTest 2: more models, new heuristics and parallel computing.
14 Nat Methods 9:772.
15 Degen R, Riavitz L, Gollner S, Vanreusel A, Plum C, Bright M (2012) Community study of tubeworm-associated
16 epizooic meiobenthos from deep-sea cold seeps and hot vents. Mar Ecol Prog Ser 468:135–148
17 Felsenstein J (1985) Confidence limits on phylogenies: an approach using the bootstrap. Evolution 39:783–791
18 Guindon S, Gascuel O (2003) A simple, fast and accurate algorithm to estimate large phylogenies by maximum
19 likelihood. Syst Biol 52:696–704

1 Guindon S, Dufayard JF, Lefort V, Anisimova M, Hordijk W, Gascuel O (2010) New algorithms and methods to estimate
2 maximum-likelihood phylogenies: assessing the performance of PhyML 3.0. Syst Biol 59:307–321
3 Karanovic I, Brandão SN (2015) Biogeography of deep-sea wood fall, cold seep and hydrothermal vent Ostracoda
4 (Crustacea), with the description of a new family and a taxonomic key to living Cytheroidea. Deep Sea Res Part II: Top
5 Stud Oceanogr 111:76–94
6 Katoh K, Misawa K, Kuma KI, Miyata T (2002) MAFFT: a novel method for rapid multiple sequence alignment based
7 on fast Fourier transform. Nucleic Acids Res 30:3059–3066
8 Katoh K, Kuma KI, Toh H, Miyata T (2005) MAFFT version 5: improvement in accuracy of multiple sequence
9 alignment. Nucleic Acids Res 33:511–518
10 Katoh K, Standley DM (2013) MAFFT multiple sequence alignment software version 7: improvements in performance
11 and usability. Mol Biol Evol 30:772–780
12 Kelley DS, Carbotte SM, Caress DW, Clague DA, Delaney JR, Gill JB, Hadaway H, Holden JF, Hooft EEE, Kellogg JP,
13 Lilley MD, Stoermer M, Toomey D, Weekly R, Wilcock WSD (2012) Endeavour Segment of the Juan de Fuca Ridge:
14 One of the most remarkable places on Earth. Oceanography 25:44–61
15 Kiel S, Goedert JL (2006) A wood-fall association from Late Eocene deep-water sediments of Washington State, USA.
16 Palaios 21:548–556
17 Kornicker LS (1991) Myodocopid Ostracoda of hydrothermal vents in the eastern Pacific Ocean. Smithson Contr Zool
18 516:1–46

Kornicker LS, Harrison-Nelson E (2005) Two new species of Ostracoda from hydrothermal vents of *Riftia pachyptila* aggregations on the East Pacific Rise (Halocypridina; Cladocopina). Zootaxa 1071:19–38

Lelièvre Y, Sarrazin J, Marticorena J, Schaal G, Day T, Legendre P, Hourdez S, Matabos M (2018) Biodiversity and trophic ecology of hydrothermal vent fauna associated with tubeworm assemblages on the Juan de Fuca Ridge. Biogeosciences 15:2629–2647

Machian-Castillo ML, Gío-Argáez FR, Escobar-Briones E (2014) Foraminíferos y ostrácodos recientes de la zona batial y abisal del sur del Golfo de México. In: Low Pfeng A, Peters Recagno EM (eds) *La frontera final: el océano profundo*. INECC, Mexico, pp. 153–173.

Maddocks RF (2005) Three new species of podocopid Ostracoda from hydrothermal vent fields at 9°50′N on the East Pacific Rise. Micropaleontology 51:345–372

Maddocks RF, Steineck PL (1987) Ostracoda from experimental wood-island habitats in the deep sea. Micropaleontology 33:318–355

Mazzini I, Gliozzi E (2000) Occurrence of fossil and Recent *Microceratina* Swanson 1980 (Ostracoda, Eucytherurinae) in the Mediterranean. Micropaleontology 46:143–152

Moon-van der Staay SY, van der Staay GWM, Guillou L, Vaulot D, Claustre H, Medlin LK (2000) Abundance and diversity of prymnesiophytes in the picoplankton community from the equatorial Pacific Ocean inferred from 18S rDNA sequences. Limnol Oceanogr 45:98–109

Nylander JAA (2004) MrModeltest v2. Program distributed by the author. Evolutionary Biology Centre, Uppsala University

Olempska E, Belka Z (2010) Hydrothermal vent myodocopid ostracods from the Eifelian (Middle Devonian) of southern Morocco. Geobis 43:519–529

Rambaut A, Suchard MA, Xie MA, Drummond AJ (2014) Tracer v1.6. Available from: http://beast.bio.ed.ac.uk/Tracer [Accessed on 12 Feb 2018]

Ronquist F, Huelsenbeck JP (2003) MrBayes 3: Bayesian phylogenetic inference under mixed models. Bioinformatics 19:1572–1574

Sarrazin J, Juniper K (1999) Biological characteristics of a hydrothermal edifice mosaic community. Mar Ecol Prog Ser 185:1–19

Sarrazin J, Robigou V, Juniper K, Delaney JR (1997) Biological and geological dynamics over four years on a high-temperature sulfide structure at the Juan de Fuca Ridge hydrothermal observatory. Mar Ecol Prog Ser 153:5–24

Steineck PL, Maddocks RF, Coles G, Whatley RC (1990) Xylophile Ostracoda in the deep sea. In: Whatley R, Maybury C (eds) *Ostracoda and Global Events*. British Micropaleontological Society Publication Series, Chapman and Hall, London, pp. 307–319

Szczechura J (1995) The ostracode genus *Xylocythere* Maddocks and Steineck, 1987, from the Middle Miocene of the Fore-Carpathian Depression, southern Poland (Central Paratethys), and its biogeographic significance. Acta Geol Pol 45:27–40

Szczechura J (2000) Age and evolution of depositional environments of the supra-evaporitic deposits in the northern, marginal part of the Carpathian Foredeep: micropalaeontologica1 evidence. Geol Quart 44:81–100

Tanaka H, Ohtsuka S (2016) Historical biogeography of the genus *Polycopissa* (Ostracoda: Myodocopa: Cladocopina), with the description and DNA barcode of the second Indo-Pacific species from the Seto Inland Sea. Mar Biodiv 46:625–640

Tanaka H, Yasuhara M (2016) A new deep-sea hydrothermal vent species of Ostracoda (Crustacea) from the Western Pacific: Implications for adaptation, endemism, and dispersal of ostracodes in chemosynthetic systems. Zool Sci 33:555–565

Van Dover CL (2002) Community structure of mussel beds at deep-sea hydrothermal vents. Mar Ecol Prog Ser 230:137–158

van Harten D (1992) Hydrothermal vent Ostracoda and faunal association in the deep sea. Deep Sea Research Part A 39: 1067–1070

van Harten D (1993) Deep sea hydrothermal vent eucytherurine Ostracoda: the enigma of the pore clusters and the paradox of the hinge. In: McKenzie KG, Jones PJ (eds) *Ostracoda in the Earth and Life Sciences*. Balkema, Rotterdam, pp. 571–580

Whatley R, Boomer I (2000) Systematic review and evolution of the early Cytheruridae (Ostracoda). J Micropalaeont 19:139–151

Xu G, Jackson, DR Bemis KG, Rona PA (2014) Time-series measurement of hydrothermal heat flux at the Grotto mound, Endeavour Segment, Juan de Fuca Ridge. Ear Planet Sci Let 404:220–231

Yamaguchi S (2003) Morphological evolution of cytherocopine ostracods inferred from 18S ribosomal DNA sequences. J Crust Biol 23:131–153

Yasuhara M, Okahashi H, Cronin TM (2009) Taxonomy of Quaternary deep-sea ostracods from the western North Atlantic Ocean. Palaeontology 52:879–931

Zeppilli D, Danovaro R (2009) Meiofaunal diversity and assemblage structure in a shallow-water hydrothermal vent in the Pacific Ocean. Aqua Biol 5:75–84

**Figure legends**

**Fig. 1** Global distribution and fossil occurrences of *Xylocythere* species. Species list and references are shown in **Table 1**. Numbers correspond with localities: 1, 190 miles southeast of Woods Hole, depth 3506 m; 2, Tongue of the Ocean, Bahama Islands, depth 2066 m; 3, off north coast of St. Croix, Virgin Islands, depth 4000 m; 4, Panama Basin, depth 3900 m; 5, this study, Juan de Fuca Ridge, depth 2196 m, details are shown in **Fig. 2**; 6, Tica and Riftia hydrothermal vent fields at 9°50'N on the East Pacific Rise, depth 2500 m; 7, Tremiti Islands, fossil; 8, Calabria, fossil; 9, Hyblean Plateau, fossil; 10, Jamnica borehole, southern Poland, fossil; 11, Goban Spur, Northeast Atlantic Ocean, Deep Sea Drilling Site S49A, fossil; 12, Queensland Plateau, southwest Pacific, Deep Sea Drilling Site 209, fossil; 13, northwest Gulf of Mexico, depth 1500 m, fossil; 14, Central equatorial Pacific, Deep Sea Drilling Site 575A, fossil; 15, western Coral Sea, depth 2023 m, fossil; 16, western Coral Sea, depth 2230 m, fossil; 17, Mason County, western Washington State, United States, fossil; 18, Santos Basin, Brazil, fossil; 20, Carolina Slope, western North Atlantic, Ocean Drilling Program Site 1055, depth 1795 m, fossil; 20, southern Gulf of Mexico, depth 2929 m, fossil.

**Fig. 2** Sampling locality. **a** location of the Juan de Fuca Ridge, northeast Pacific and the seven segments. A rectangular indicating the Main Endeavour Field. **b** Bathymetric map and the positions of hydrothermal vent edifices of the Main Endeavour Field (Endeavour, Juan de Fuca Ridge). A star indicating the Grotto hydrothermal edifice, the type locality of *Xylocythere sarrazinae* sp. nov.

**Fig. 3** Scatter plots of valves of *Xylocythere sarrazinae* sp. nov. from the type locality. Triangle and circle indicate male and female, respectively.

**Fig. 4** External view of valves of *Xylocythere sarrazinae* sp. nov., male, holotype (UMUT RA32930). **a** internal lateral view of left valve; **b** internal lateral view of right valve. *Scale bar* 100 µm.

**Fig. 5** Scanning electron microscope images of valves of *Xylocythere sarrazinae* sp. nov. **a**, **b** male paratype (UMUT RA32931); **c**, **d** male paratype (UMUT RA32932); **e**, **f** female paratype (UMUT RA32937); **g** male paratype (UMUT RA32933); **h** female paratype (UMUT RA32938): **a** external lateral view of right valve; **b** external lateral view of left valve; **c** internal lateral view of right valve; **d** internal lateral view of left valve; **e** external lateral view of right valve; **f** external lateral view of left valve; **g** dorsal view of carapace, a posteriorly-directed postero-ventral spine of both valves are broken; **h** dorsal view of carapace. *Scale bar* 100 µm.

**Fig. 6** Scanning electron microscope images of valves of *Xylocythere sarrazinae* sp. nov., internal lateral view, male paratype (UMUT RA32932). **a** hingement of left valve; **b** hingement of right valve; **c** posterior element of left valve; **d** posterior element of right valve; **e** anterior element of left valve; **f** anterior element of right valve; **g** internal view of pore clusters; **h** adductor muscle scars. *Scale bars* 100 µm (**a**, **b**), 50 µm (**c**–**h**).

**Fig. 7** *Xylocythere sarrazinae* sp. nov. **a**, **b** male holotype (UMUT RA32930); **c**–**f** male paratype (UMUT RA32932); **g**–**j** male paratype (UMUT RA32934). **a** antennula; **b** antenna; **c** mandibula; **d** mandibula, first podomere of endopodite; **e** mandibula, coxal endites; **f** maxillula, branchial plate and refluxed setae; **g** maxillula, palp and endites (without setae); **h** maxillula, dorsal endite; **i** maxillula, middle endite; **j** maxillula, ventral endite. Abbreviations and numbers at tips of setae indicate the segments of insertion: *1en* to *4en*, first to fourth endopodite; *4* to *6*, fourth to sixth podomere. *Scale bars* 50 µm.

**Fig. 8** *Xylocythere sarrazinae* sp. nov. **a**–**c** male paratype (UMUT RA32932); **d**, **e** male paratype (UMUT RA32935). **a** fifth limb; **b** sixth limb; **c** seventh limb; **d** brush-shaped organ; **e** head capsule in left lateral view. *Scale bars* 50 µm

**Fig. 9** *Xylocythere sarrazinae* sp. nov. **a** male copulatory organ and posterior body, holotype (UMUT RA32930); **b** female copulatory organ and posterior body, paratype (UMUT RA32937). *Abbreviations*: *cp* copulatory process, *dp* distal process, *lra* lower ramiform appendage, *ur* upper ramus. *Scale bars* 50 µm.

**Fig. 10 a** Maximum likelihood (ML) tree based on 18S rDNA sequences using the GTR+I+G model of nucleotide substitution. The number of branches indicate bootstrap value (ML) and posterior probabilities (Bayesian inference). Scale bar indicates substitutions per site. The clade including *Xylocythere sarrazinae* sp. nov. indicated by gray box. **b** the cladogram of clade including *X. sarrazinae* sp. nov. extracted from **Fig. 9a**. Scanning electron microscope image shows left valves in external view: the upper row, *X. sarrazinae* sp. nov., *Cytheropteron* sp., *Semicytherura sagittiformis* Yamada and Tanaka, 2011; the lower row, *Paracytherois chukchiensis* Joy and Clark, 1977, *Obesostoma obesum* (Schornikov, 1974).

**Table 1** Species list of living and fossil *Xylocythere*. Numbers correspond with locality are indicated in **Fig. 1**.

*Abbreviations*: E, Eocene; H, Holocene; HV, hydrothermal vent; M, Miocene; Og, Oligocene; Ps, Pleistocene; WF, wood fall.

| | Late E | Late Og | Early M | Middle M | Lare M | Eearly Ps | Late Ps | H | Recent HV | Recent WF | References |
|---|---|---|---|---|---|---|---|---|---|---|---|
| *Xylocythere trunerae* Maddocks and Steineck, 1987 | | | | | | | | | | 1, 2, 3 | Maddocks and Steineck (1987) |
| *X. pointillissima* Maddocks and Steineck, 1987 | | | | | | | | | | 1, 2, 3 | Maddocks and Steineck (1987) |
| *X. rimosa* Maddocks and Steineck, 1987 | | | | | | | | | | 4 | Maddocks and Steineck (1987) |
| *X. tridentis* Maddocks and Steineck, 1987 | | | | | | | | | | 1 | Maddocks and Steineck (1987) |
| *X. sarrazinae* **sp. nov.** | | | | | | | | | 5 | | This study |
| *X. vanharteni* Maddocks, 2005 | | | | | | | | | 6 | | Van Harten (1992, 1993); Maddocks (2005) |
| *X. producta* (Colalongo and Pasini, 1980) | | | | 7, 9 | | 8 | | | | | Colalongo and Pasini (1980); Dall'Antonia (2003) |
| *X. carpathica* Szczechura, 1995 | | | | 10 | | | | | | | Szczechura (1995, 2000) |
| *X.* sp. 1 from Steineck et al. (1990) | | 11 | | | | | | | | | Steineck et al. (1990) |
| *X.* sp. 2 from Steineck et al. (1990) | | | | 12 | | | | | | | Steineck et al. (1990) |
| *X.* sp. 3 from Steineck et al. (1990) | | | | | | | | 13 | | | Steineck et al. (1990) |
| *X.* sp. 4 from Steineck et al. (1990) | | | | | | | | 13 | | | Steineck et al. (1990) |
| *X.* sp. 5 from Steineck et al. (1990) | | | | | 11 | | | | | | Steineck et al. (1990) |

| | | | | |
|---|---|---|---|---|
| *X*. sp. 6 from Steineck et al. (1990) | | | 13 | Steineck et al. (1990) |
| *X*. sp. 7 from Steineck et al. (1990) | | 14 | | Steineck et al. (1990) |
| *X*. sp. from Corrège (1993) | | | 15, 16 | Corrège (1993) |
| *X*. sp. from Kiel and Goedert (2006) | 17 | | | Kiel and Goedert (2006) |
| *X*. sp. from Bergue and Coimbra (2008) | | | 18 | Bergue and Coimbra (2008) |
| *X*. sp. from Yasuhara et al. (2009) | | | 19 | Yasuhara et al. (2009) |
| *X*. sp. from Machian-Castillo et al. (2014) | | | 20 | Machian-Castillo et al. (2014) |

**Table 2** Dimension of valves of *Xylocythere sarrazinae* sp. nov. from the type locality.

| | | Length (μm) | | | Height (μm) | | |
|---|---|---|---|---|---|---|---|
| | | Mean | Observed range | *N* | Mean | Observed range | *N* |
| Male | RV | 542 | 528–549 | 7 | 257 | 247–263 | 7 |
| | LV | 542 | 530–556 | 6 | 262 | 254–267 | 6 |
| Female | RV | 557 | 541–576 | 12 | 272 | 266–280 | 12 |
| | LV | 555 | 538–578 | 10 | 277 | 270–284 | 10 |

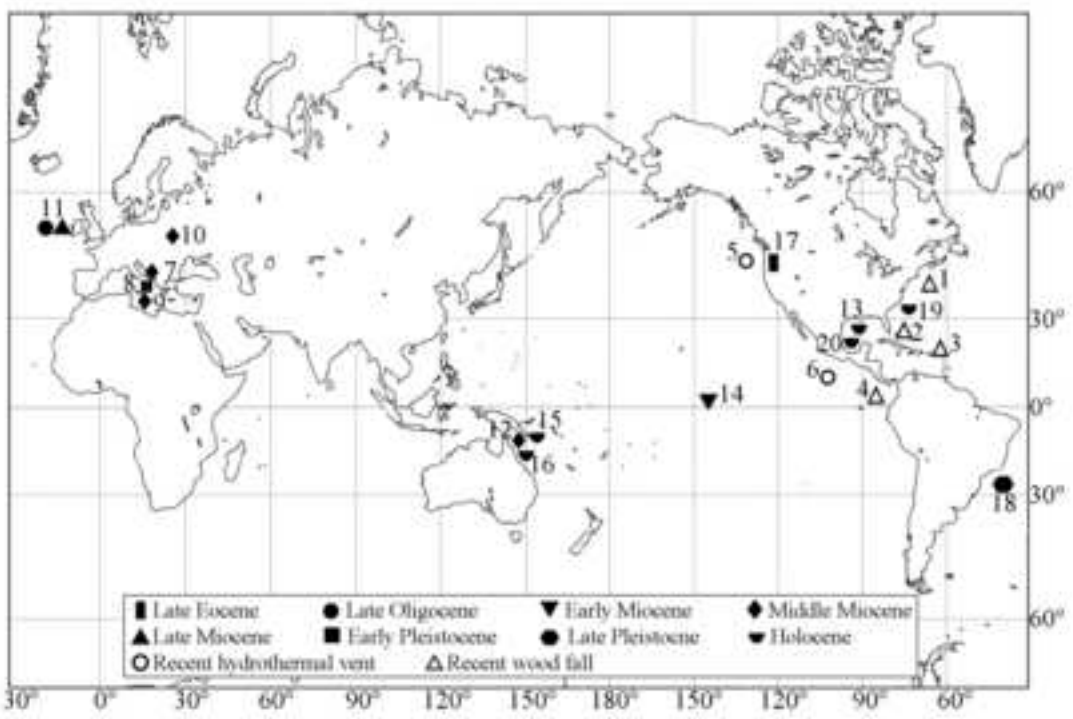


Fig. 1

Figure 2

Click here to access/download;Figure;Figure 2.jpg

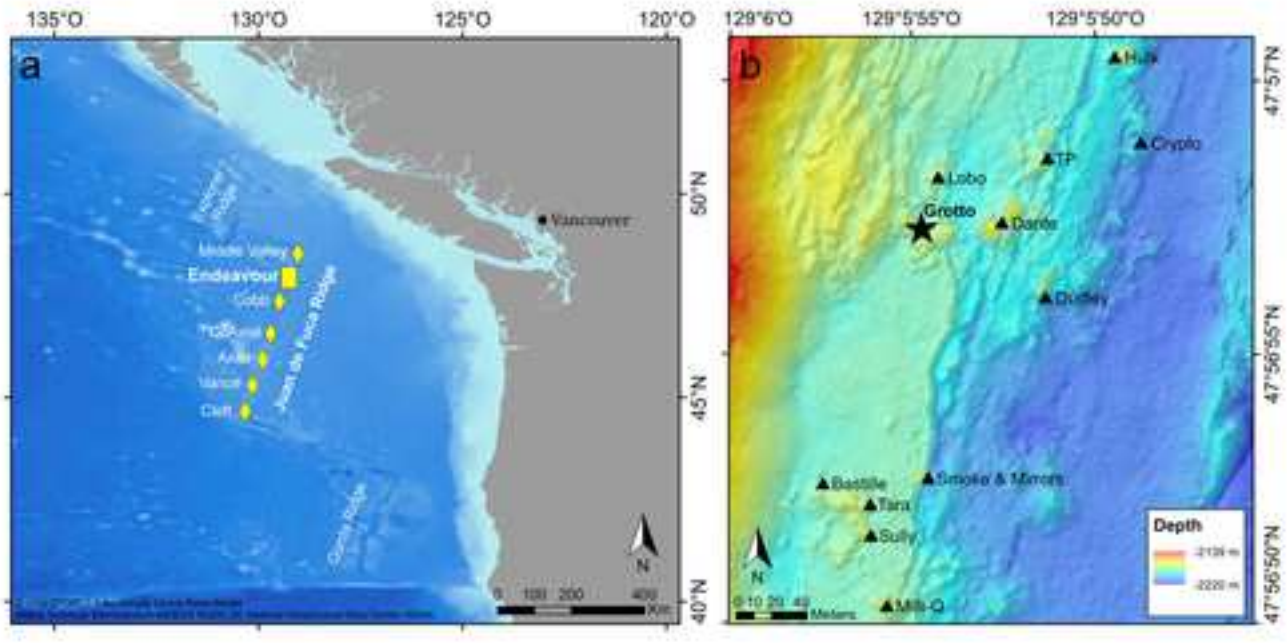


Fig. 2

Figure 3



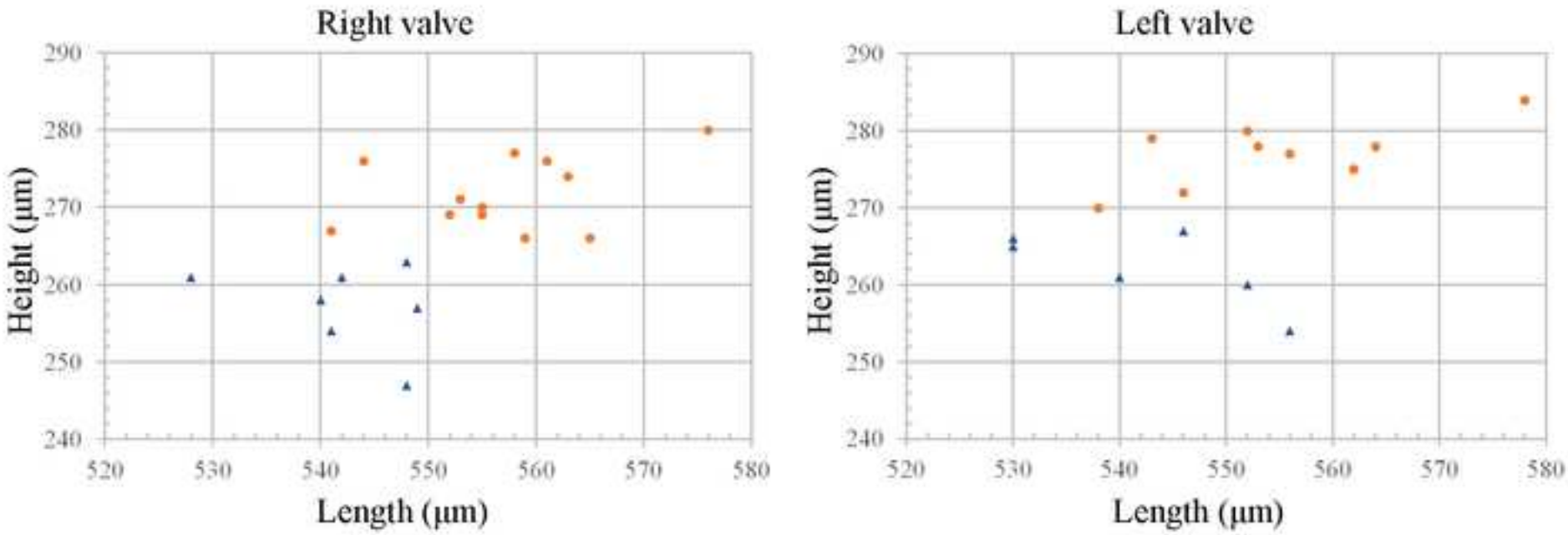

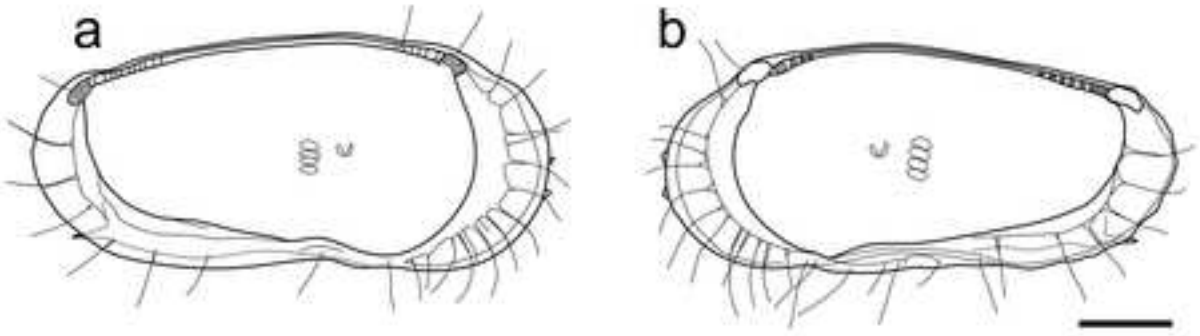


Fig. 4

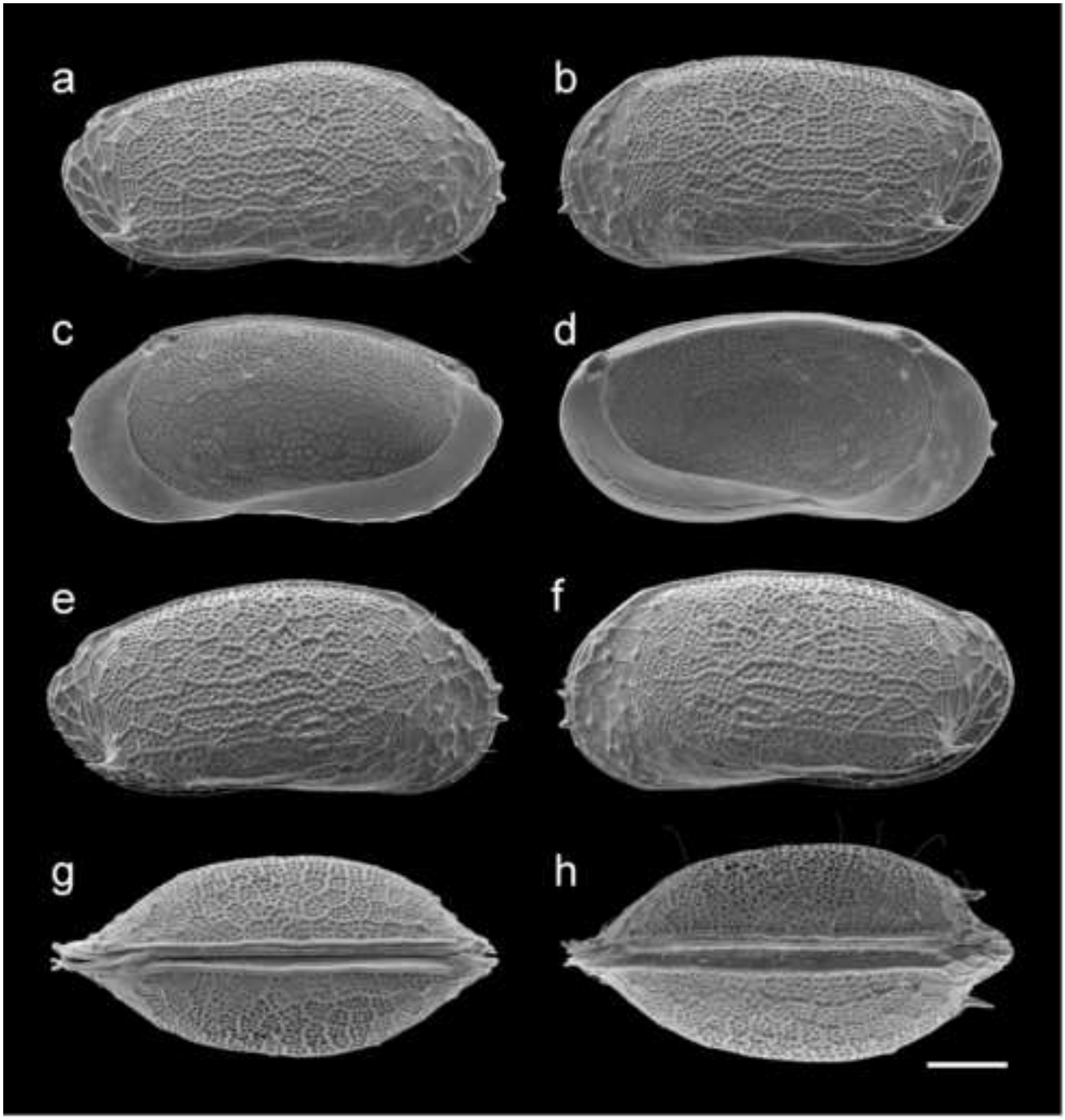


Fig. 5

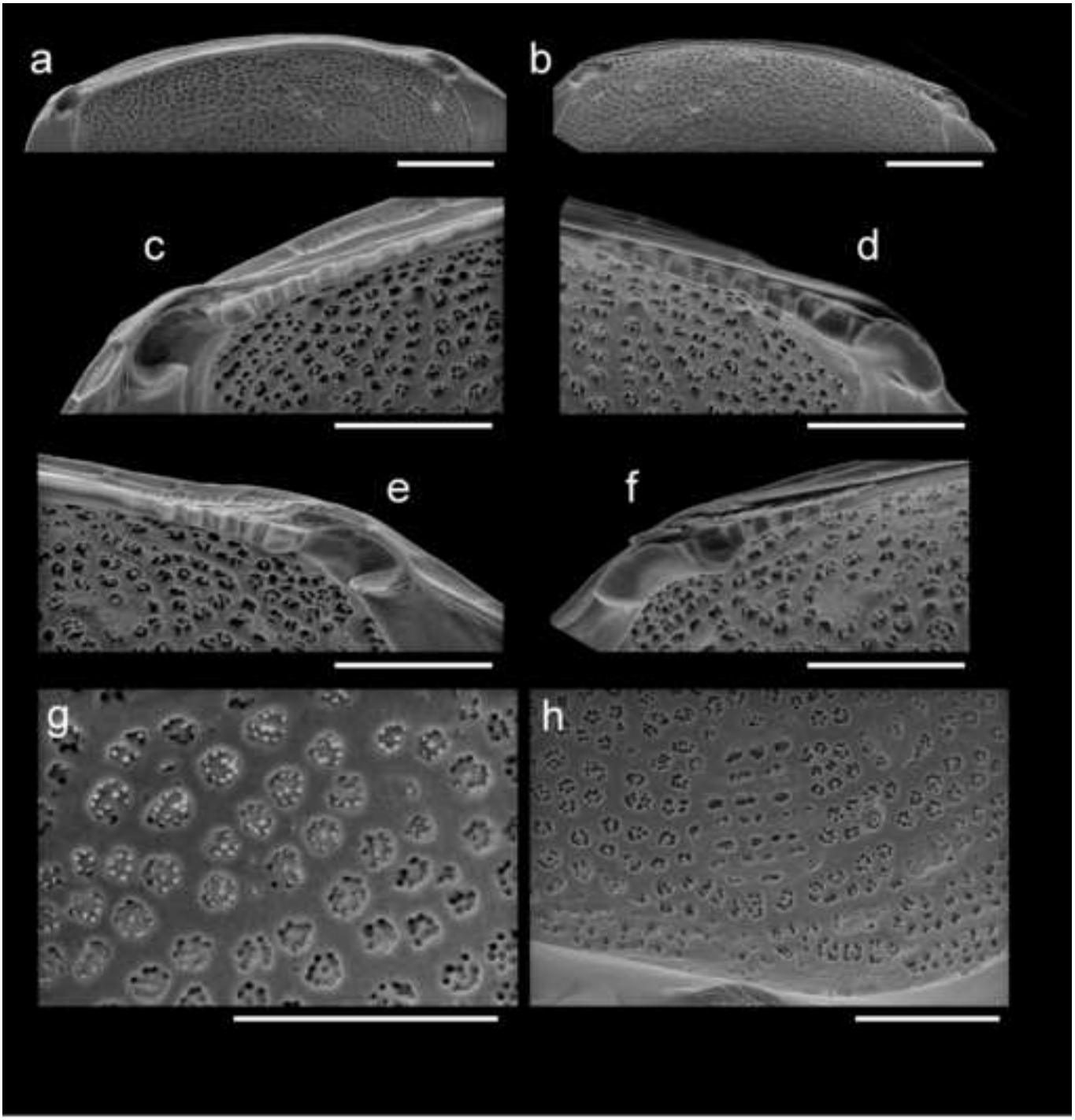


Fig. 6

Figure 7

Click here to access/download;Figure;Figure 7.jpg

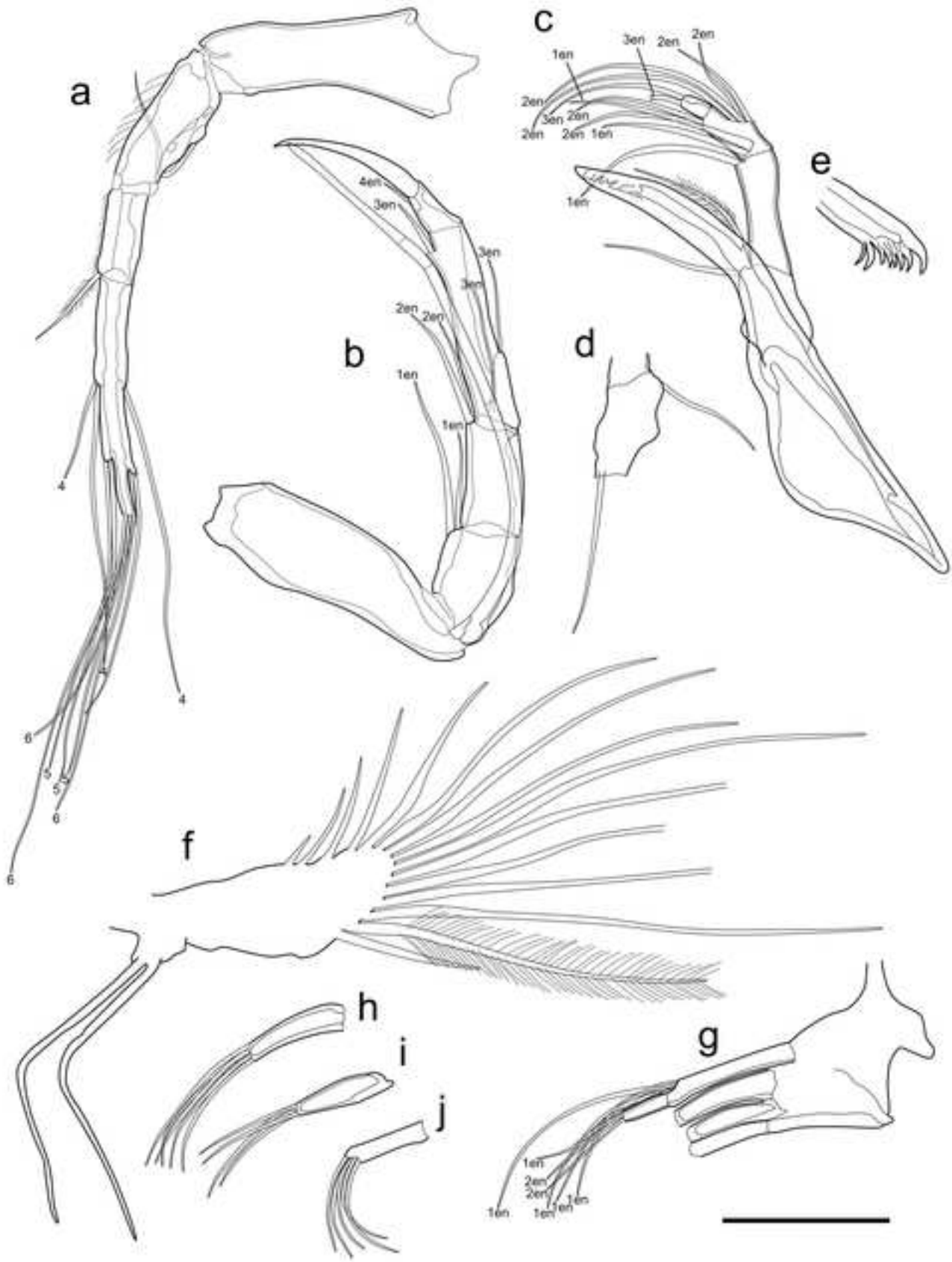


Fig. 7

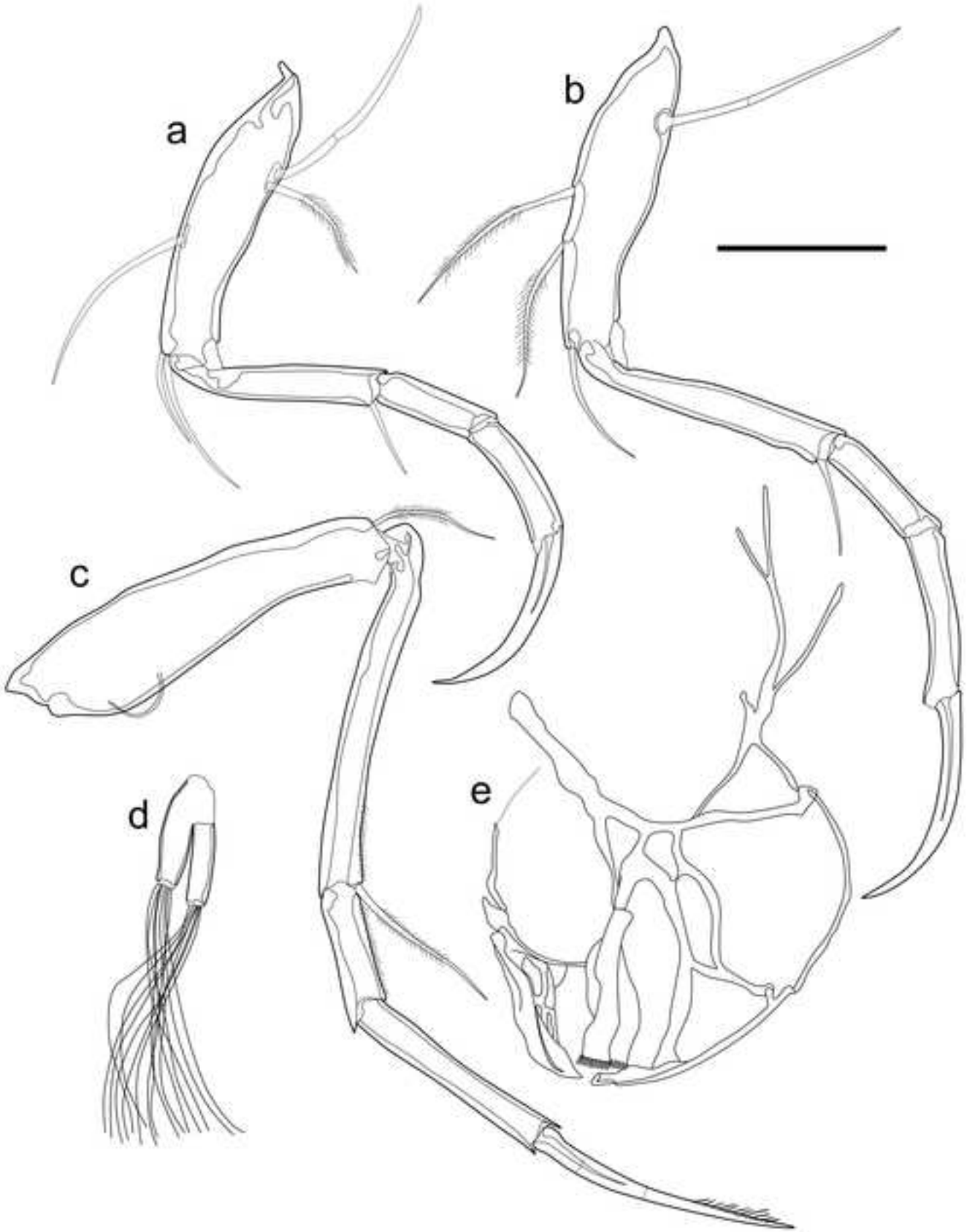


Fig. 8

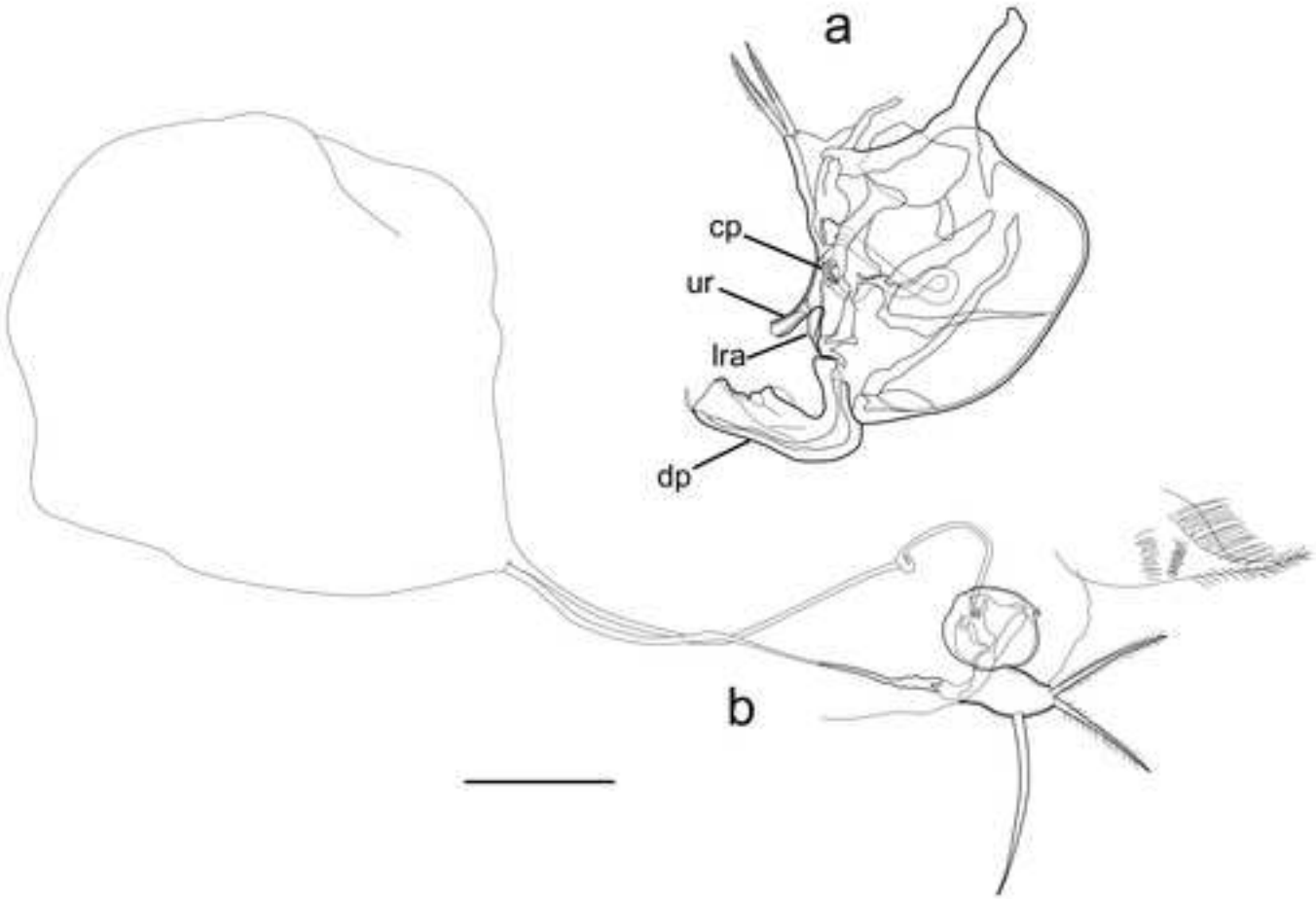


Fig. 9

Figure 10

Click here to access/download;Figure;Figure 10.jpg

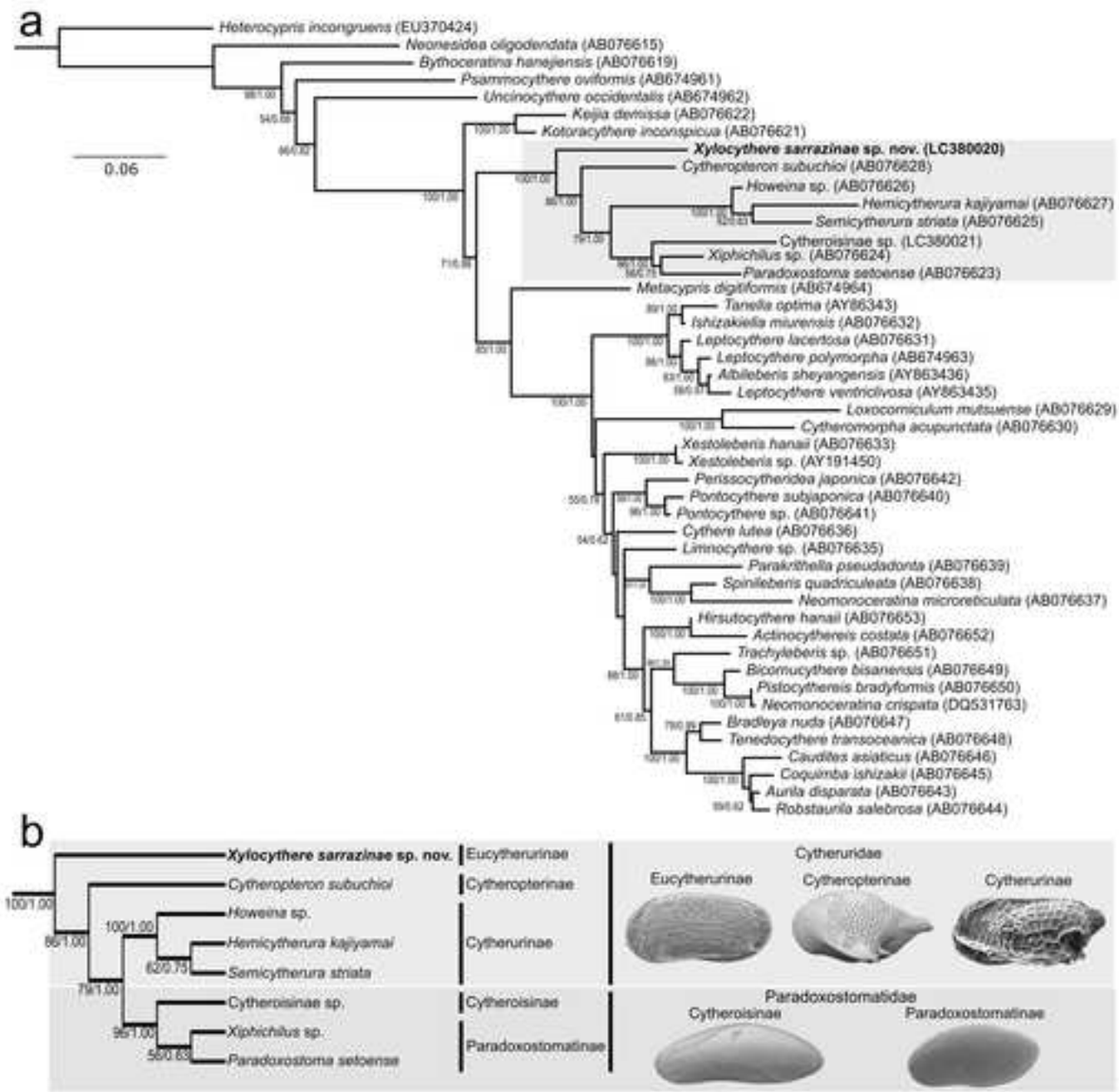


Fig.10

Table 1

| | Late E | Late Og | Early M | Middle M | Lare M | Eearly Ps | Late Ps | H | Recent HV | Recent WF | References |
|---|---|---|---|---|---|---|---|---|---|---|---|
| *Xylocythere trunerae* Maddocks and Steineck, 1987 | | | | | | | | | | 1, 2, 3 | Maddocks and Steineck (1987) |
| *X. pointillissima* Maddocks and Steineck, 1987 | | | | | | | | | | 1, 2, 3 | Maddocks and Steineck (1987) |
| *X. rimosa* Maddocks and Steineck, 1987 | | | | | | | | | | 4 | Maddocks and Steineck (1987) |
| *X. tridentis* Maddocks and Steineck, 1987 | | | | | | | | | | 1 | Maddocks and Steineck (1987) |
| *X. sarrazinae* **sp. nov.** | | | | | | | | | 5 | | This study |
| *X. vanharteni* Maddocks, 2005 | | | | | | | | | 6 | | Van Harten (1992, 1993); Maddocks (2005) |
| *X. producta* (Colalongo and Pasini, 1980) | | | | 7, 9 | | 8 | | | | | Colalongo and Pasini (1980); Dall'Antonia (2003) |
| *X. carpathica* Szczechura, 1995 | | | | 10 | | | | | | | Szczechura (1995, 2000) |
| *X.* sp. 1 from Steineck et al. (1990) | | 11 | | | | | | | | | Steineck et al. (1990) |
| *X.* sp. 2 from Steineck et al. (1990) | | | | 12 | | | | | | | Steineck et al. (1990) |
| *X.* sp. 3 from Steineck et al. (1990) | | | | | | | | 13 | | | Steineck et al. (1990) |
| *X.* sp. 4 from Steineck et al. (1990) | | | | | | | | 13 | | | Steineck et al. (1990) |
| *X.* sp. 5 from Steineck et al. (1990) | | | | | 11 | | | | | | Steineck et al. (1990) |
| *X.* sp. 6 from Steineck et al. (1990) | | | | | | | | 13 | | | Steineck et al. (1990) |
| *X.* sp. 7 from Steineck et al. (1990) | | | 14 | | | | | | | | Steineck et al. (1990) |
| *X.* sp. from Corrège (1993) | | | | | | | | 15, 16 | | | Corrège (1993) |
| *X.* sp. from Kiel and Goedert (2006) | 17 | | | | | | | | | | Kiel and Goedert (2006) |
| *X.* sp. from Bergue and Coimbra (2008) | | | | | | | 18 | | | | Bergue and Coimbra (2008) |
| *X.* sp. from Yasuhara et al. (2009) | | | | | | | | 19 | | | Yasuhara et al. (2009) |
| *X.* sp. from Machian-Castillo et al. (2014) | | | | | | | | 20 | | | Machian-Castillo et al. (2014) |

Table 2. Dimension of valves of *Xylocythere sarrazinae* sp. nov. from the type locality.

| | | Length (μm) | | | Height (μm) | | |
|---|---|---|---|---|---|---|---|
| | | Mean | Observed range | *N* | Mean | Observed range | *N* |
| Male | RV | 542 | 528–549 | 7 | 257 | 247–263 | 7 |
| | LV | 542 | 530–556 | 6 | 262 | 254–267 | 6 |
| Female | RV | 557 | 541–576 | 12 | 272 | 266–280 | 12 |
| | LV | 555 | 538–578 | 10 | 277 | 270–284 | 10 |

**Zoobank registration number of new species**

urn:lsid:zoobank.org:act:66E0D33D-CAB8-4C4F-8758-D7E95A7CAC69

**Data availability statement**

Sequence data of *Xylocythere sarrazinae* sp. nov. that support the findings of this study have been deposited in GenBank with the accession codes LC380020 (https://www.ncbi.nlm.nih.gov/nuccore/LC380020.1)